Pergamon

Int. J. Mech. Sci. Vol. 37, No. 2, pp. 197–219, 1995
Elsevier Science Ltd
Printed in Great Britain
0020-7403/95 $9.50 + 0.00

0020-7403(94)00045-X

ESTIMATION OF LINEARIZED DYNAMIC CHARACTERISTICS OF BEARINGS USING SYNCHRONOUS RESPONSE

JUHN-HORNG CHEN and AN-CHEN LEE

Department of Mechanical Engineering, National Chiao Tung University, 1001 Ta Hsueh Road, Hsinchu 30049, Taiwan, R.O.C.

(*Received* 1 *June* 1993; *and in revised form* 14 *April* 1994)

Abstract—This paper presents a new method for estimating linearized dynamic characteristics of bearings using *a priori* information about the rotor. The rotor-bearing systems considered here are composed of a flexible shaft, which may be changed stepwise along the axial direction, and multiple rigid disks supported on anisotropic bearings. The main feature of this estimation technique is that it eliminates the need to measure the external input force. Since the system considered here is driven by an unbalance force, the steady state of the rotor will contain only a synchronous frequency component. By applying a Fourier transform to the measured displacement, we can obtain the coefficients of the sine and cosine terms with respect to the synchronous frequency. Finally, we formulate the normal equation by using the relations between these coefficients and the known system parameters; the characteristics of the bearings are then estimated by the least-squares method. The theoretical development of the method is presented together with simulation and experimental results.

NOTATION

m	mass
ρA	mass per unit length
I, J	diametric and polar mass moments of inertias
EI	flexural rigidity
L, l	length of shaft and shaft element
Ω	spin speed
z	the position coordinate along the shaft
$c^{b}_{xx}\ k^{b}_{xx}$	etc. damping and stiffness coefficients of bearings
C^{b}_{i}, K^{b}_{i}	damping and stiffness matrices of ith bearing
q^{e}, q^{d}, q^{b}, q	degree of freedom vectors of shaft element, disk, bearing and global system
ϕ_x, ϕ_y	interpolation functions of x and y directions
$\mathbf{M}^{s}_{i}, \mathbf{M}^{r}_{i}, \mathbf{G}^{e}_{i}, \mathbf{K}^{e}_{i}$	translation mass, rotation mass, gyroscopic and stiffness matrices of ith element
$\mathbf{M}^{d}_{i}, \mathbf{G}^{d}_{i}, \mathbf{K}^{d}_{i}$	mass, gyroscopic and stiffness matrices of ith disk
f^{d}_{i}	forcing vector acting on ith node including external and disk unbalance force
$\mathbf{M}, \mathbf{C}, \mathbf{K}$	global mass, damping and stiffness matrices
f_x, f_y	distributed forcing functions in the x and y directions
f_{xi}, f_{yi}	forces acting on ith node in x and y directions
T_x, T_y	bending moments acting on ith node in x and y directions

Superscripts

$(\cdot)^{*}$	submatrix and composed of first two rows of matrix $(\cdot)$
$(\cdot)^{\#}$	submatrix and composed of first four rows of matrix $(\cdot)$
$(\cdot)^{t}$	transpose matrix of matrix $(\cdot)$
b, d, e	superscripts for bearing, disk, and shaft element

1. INTRODUCTION

During the past decade, many experimenters have devoted attention to identifying the dynamic coefficients of bearings experimentally. Burrow and Stanway [1] used PRBSs (Pseudo-random-binary sequences) as inputs and obtained the eight linearized coefficients of journal bearings using multiple regression analysis. The same approach was applied to estimate the two velocity coefficients of a squeeze-film bearing by sampled observations from laboratory experiments [2], where the motion of the journal in the vertical and horizontal directions were assumed to be uncoupled. Burrows and Sahinkaya [3] developed a frequency-domain algorithm to yield estimates of the eight oil-film coefficients by

using a Schroeder-phased harmonic excitation, and showed that the technique was more efficient than the time-domain algorithm described in earlier work. Stanway [4] used a nonlinear filter to estimate the four damping coefficients associated with a squeeze-film isolator from time-series records of the displacement responses to synchronous excitation. In more recent work, Shahinkaya and Burrows [5] developed a time-domain scheme for estimating the coefficients of an oil-film bearing from the out-of-unbalance responses. They showed that only four coefficients could be estimated if the signals contained the same frequency. Lee and Hong [6] proposed an identification scheme for estimating the coefficients of a bearing from the out-of-unbalance responses and showed the eight coefficients could be fully identified by using four sensors at two locations for two different unbalance conditions. The system considered in these studies [1–6] comprised a rigid rotor supported by two short journal bearings. Through the use of *a priori* information about the inertial properties of the rigid rotor, the coefficients of the bearings can be estimated by measuring the input force and responses. In reality, however, the bearings are anisotropic in character and their stiffness and damping coefficients are functions of the speed of rotation. For a flexible shaft in a real case, the results obtained by these approaches may be acceptable for a rotor running at a speed under the first flexible mode, but at higher flexible modes there may be a significant error in the estimates produced by these methods. In addition to the above limitation, most of these approaches [1–5] stipulate that the system be supported symmetrically by two identical bearings, and in general this restriction is not compatible with real situations. Kim and Kwak [7] proposed a method based on the Timoshenko beam theorem for identifying the stiffness and damping coefficients of isotropic bearings by using the transfer matrix method. But this method can only be applied to static situations (nonrotating condition); that is, the changeable characteristics of the bearings at different speeds of rotation are not addressed.

The rotor-bearing systems considered here are composed of a flexible shaft that may be changed stepwise along the axial direction and multiple rigid disks supported on anisotropic bearings. Each bearing can be represented by eight linearized parameters, i.e. four stiffness and four damping coefficients. The equations of motion can be obtained by using the extended Hamilton's principle to yield partial differential equations. Through the finite element method, the partial differential equations are discretized in space so that they have finite dimensions. This paper presents a coherent strategy for estimating linearized characteristics of bearings based on *a priori* information about the rotor. The main feature of this identification technique is that it eliminates the need to measure the external input force. Since the system considered here is driven by an unbalance force, the steady state of the rotor will contain only a synchronous frequency component. By applying a Fourier transform to the measured displacement, we can obtain the coefficients of the sine and cosine terms. Finally, we formulate the normal equation by using the relations between these coefficients and the known system parameters; the characteristics of the bearings are then estimated by the least-squares method.

2. EQUATIONS OF MOTION

Consider a flexible rotor system consisting of D disks and B bearings, as shown in Fig. 1. For simplicity, assume that discontinuity in stiffness, damping caused by the bearing, and inertia caused by the disks are well represented by a train of delta functions along the shaft axis. The equations of motion, including the effects of gyroscopic and rotary inertia in the inertial coordinates, can be obtained as follows [8]:

$$\begin{aligned}
&\rho A(z)\frac{\partial^2 x}{\partial t^2} - \Omega\frac{\partial}{\partial z}\left[J(z)\frac{\partial^2 y}{\partial z\partial t}\right] - \frac{\partial}{\partial z}\left[I(z)\frac{\partial^3 x}{\partial t^2\partial z}\right] + \frac{\partial^2}{\partial z^2}\left[EI(z)\frac{\partial^2 x}{\partial z^2}\right] \\
&\quad + k^{b}_{xx}(z)\,x + k^{b}_{xy}(z)\,y + c^{b}_{xx}(z)\,\dot{x} + c^{b}_{xy}(z)\,\dot{y} = f_x(z,t) \\
&\rho A(z)\frac{\partial^2 y}{\partial t^2} + \Omega\frac{\partial}{\partial z}\left[J(z)\frac{\partial^2 x}{\partial z\partial t}\right] - \frac{\partial}{\partial z}\left[I(z)\frac{\partial^3 y}{\partial t^2\partial z}\right] + \frac{\partial^2}{\partial z^2}\left[EI(z)\frac{\partial^2 y}{\partial z^2}\right] \\
&\quad + k^{b}_{yx}(z)\,x + k^{b}_{yy}(z)\,y + c^{b}_{yx}(z)\,\dot{x} + c^{b}_{yy}(z)\,\dot{y} = f_y(z,t)
\end{aligned} \tag{1}$$

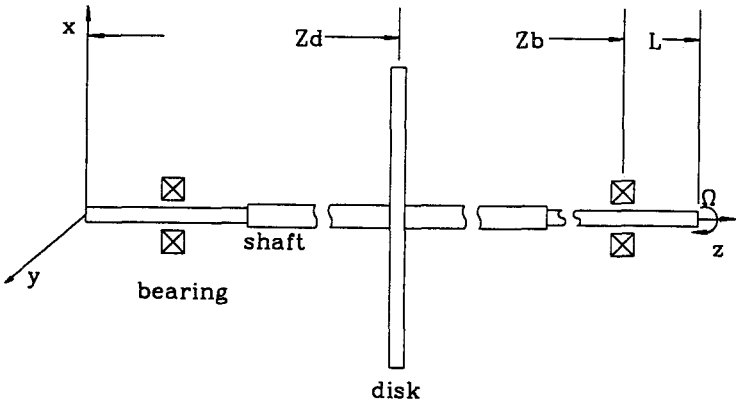

Fig. 1. A general rotor-bearing system.

where $0 < z < L$ and

$$\rho A(z) = \rho^{e} A^{e}(z) + \sum_{i=1}^{D} m_i^{d}\,\delta(z - z_i^{d})$$

$$I(z) = I^{e}(z) + \sum_{i=1}^{D} I_i^{d}\,\delta(z - z_i^{d}) \qquad J(z) = J^{e}(z) + \sum_{i=1}^{D} J_i^{d}(\delta(z - z_i^{d})$$

$$k_{xx}^{b}(z) = \sum_{i=1}^{B} k_{xxi}^{b}\,\delta(z - z_i^{b}) \qquad k_{xy}^{b}(z) = \sum_{i=1}^{B} k_{xyi}^{b}\,\delta(z - z_i^{b})$$

$$k_{yx}^{b}(z) = \sum_{i=1}^{B} k_{yxi}^{b}\,\delta(z - z_i^{b}) \qquad k_{yy}^{b}(z) = \sum_{i=1}^{B} k_{yyi}^{b}\,\delta(z - z_i^{b})$$

$$c_{xx}^{b}(z) = \sum_{i=1}^{B} c_{xxi}^{b}\,\delta(z - z_i^{b}) \qquad c_{xy}^{b}(z) = \sum_{i=1}^{B} c_{xyi}^{b}\,\delta(z - z_i^{b})$$

$$c_{yx}^{b}(z) = \sum_{i=1}^{B} c_{yxi}^{b}\,\delta(z - z_i^{b}) \qquad c_{yy}^{b}(z) = \sum_{i=1}^{B} c_{yyi}^{b}\,\delta(z - z_i^{b})$$

The system parameters of the rotor-bearing system shown in Eqn (1) may be complicated functions of the spatial variables for a system configuration, so an exact parameter identification may not be feasible. This implies that the direct use of Eqn (1) for identification purposes is not practical. Since in practice the diameter of a shaft often changes stepwise along the axial direction, we propose an identification approach based on the finite element method.

Let q_i^{e} be the nodal displacement vector of the ith element with eight degrees of freedom, four degrees of freedom of displacement in the x and y directions and four of rotation about the x and y coordinates (see Fig. 2). The term nodal derives from the fact that in finite

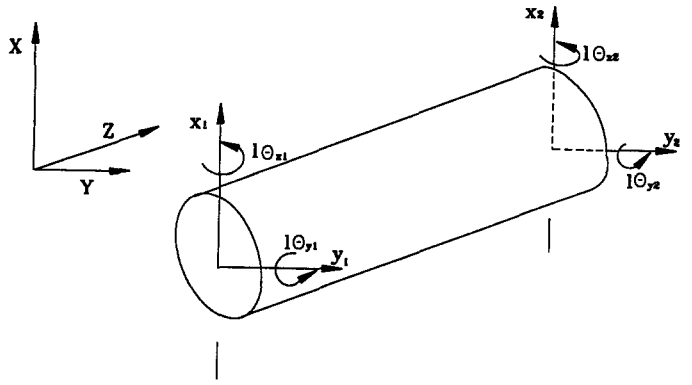

Fig. 2. Nodal coordinates of the shaft element.

element terminology the boundary points are called nodal. Let ϕ_x and ϕ_y be the interpolation functions of the x and y coordinates, which are the lowest degree admissible polynomials, i.e. the cubic spline. In particular, we have

$$q_i^e = [x_i \;\; y_i \;\; l\theta_{yi} \;\; l\theta_{xi} \;\; x_{i+1} \;\; y_{i+1} \;\; l\theta_{y(i+1)} \;\; l\theta_{x(i+1)}]^t \tag{2}$$

$$\phi_x = [\phi_{1x} \;\; 0 \;\; \phi_{2x} \;\; 0 \;\; \phi_{3x} \;\; 0 \;\; \phi_{4x} \;\; 0]^t \tag{3}$$

$$\phi_y = [0 \;\; \phi_{1y} \;\; 0 \;\; -\phi_{2y} \;\; 0 \;\; \phi_{3y} \;\; 0 \;\; -\phi_{4y}]^t \tag{4}$$

$$x = \phi_x^t \; q_i^e \quad y = \phi_y^t \; q_i^e$$

$$\begin{bmatrix} x \\ y \end{bmatrix} = \begin{bmatrix} \phi_x^t \\ \phi_y^t \end{bmatrix} q_i^e = \phi^t q_i^e \quad \phi = [\phi_x, \phi_y]_{8\times 2} \tag{5}$$

where

$$\phi_{1x} = \phi_{1y} = 2\xi^3 - 3\xi^2 + 1; \quad \phi_{2x} = \phi_{2y} = \xi^3 - 2\xi^2 + \xi$$

$$\phi_{3x} = \phi_{3y} = -2\xi^3 + 3\xi^2; \quad \phi_{4x} = \phi_{4y} = \xi^3 - \xi^2 \quad 0 \leqslant \xi \leqslant 1 \tag{6}$$

in which ξ denotes the non-dimensional natural coordinate for the ith element and equals $(z - z_i)/l$.

By using Galerkin's formulation of the weighted residual method [9], we obtain the element mass, damping and stiffness matrices for the shaft:

$$\mathbf{M}_i^s = \int_{(i-1)l}^{il} \phi(z) \cdot \rho_i^e A_i^e \phi^t(z)\, dz$$

$$= l\rho^e A_i^e \int_0^1 (\phi_x \phi_x^t + \phi_y \phi_y^t)\, d\xi = m_i^s \, L_s \quad \text{(translation mass matrix)}$$

$$\mathbf{M}_i^r = \int_{(i-1)l}^{il} \phi(z) \cdot \{\rho_i^e A_i^e \phi^t(z) - [I_i^e \phi^{tv}(z)]'\}\, dz$$

$$= I_i^e/l^2 \int_0^1 (\phi_x' \phi_x^{t\prime} + \phi_y' \phi_y^{t\prime})\, d\xi = m_i^r \quad L_r \quad \text{(rotatory mass matrix)}$$

$$\mathbf{G}_i^c = \int_{(i-1)l}^{il} \phi(z) \cdot \Omega \begin{bmatrix} -(J_i^e \phi_y^{t\prime}(z))' \\ J_i^e \phi_x^t(z)]' \end{bmatrix} dz$$

$$= \Omega J_i/l^2 \int_0^1 (\phi_y' \phi_x^{t\prime}\, d\xi - \phi_x' \phi_y^{t\prime})\, d\xi = c_i^e \; L_c \quad \text{(gyroscopic matrix)}$$

$$\mathbf{K}_i^e = \int_{(i-1)l}^{il} \phi(z) \cdot \{[E_i^e I_i^e \phi^{tv}(z)]''\}\, dz$$

$$= E_i I_i^e/l^3 \int_0^1 (\phi_x'' \phi_x^{tv} + \phi_y'' \phi_y^{tv})\, d\xi = k_i^e \; L_k \quad \text{(stiffness matrix)} \tag{7}$$

where $m_i^s = l\rho^e A_i^e$, $m_i^r = I_i^e/l^2$, $c_i^e = \Omega J_i^e/l^2$, and $k_i^e = E_i I_i^e/l^3$ are scalar and depend on the properties of the rotor. Since interpolation functions ϕ_y and ϕ_x are given, the following 8×8 known local matrices $\mathbf{L}_s = \int_0^1 (\phi_x \phi_x^t + \phi_y \phi_y^t)d\xi$, $\mathbf{L}_r = \int_0^1 (\phi_x' \phi_x^{tv} + \phi_y' \phi_y^{t\prime})\, d\xi$, $\mathbf{L}_c = \int_0^1 (\phi_y' \phi_x^{tv}\, d\xi - \phi_x \phi_y^{tv})d\xi$, and $\mathbf{L}_k = \int_0^1 (\phi_x'' \phi_x^{tv} + \phi_y'' \phi_y^{tv})\, d\xi$ can be obtained as shown in Appendix A.

The ith thin rigid disk at the jth node has an equation of the following form:

$$\mathbf{M}_i^d \ddot{q}_j^d + \mathbf{G}_i^d \dot{q}_j^d = f_j^d \tag{8}$$

where

$$\mathbf{M}_i^d = \begin{bmatrix} m_i^d & & & 0 \\ & m_i^d & & \\ & & I_i^d/l^2 & \\ 0 & & & I_i^d/l^2 \end{bmatrix} \quad \mathbf{G}_i^d = \Omega \begin{bmatrix} 0 & & & \\ & 0 & & 0 \\ & & 0 & -J_i^d/l^2 \\ 0 & & -J_i^d/l^2 & 0 \end{bmatrix}$$

$$q_j^d = [x_j, \; y_j, \; l\theta_{y_j}, \; l\theta_{x_j}]^t$$

The ith linearized bearing at the jth node is represented in the direct stiffness and damping [10] approach as

$$\begin{bmatrix} c^{b}_{xxi} & c^{b}_{xyi} \\ c^{b}_{yxi} & c^{b}_{yyi} \end{bmatrix} \dot{q}^{b}_{j} + \begin{bmatrix} k^{b}_{xxi} & k^{b}_{xyi} \\ k^{b}_{yxi} & k^{b}_{yyi} \end{bmatrix} q^{b}_{j} = \mathbf{C}^{b}_{i}\dot{q}^{b}_{j} + \mathbf{K}^{b}_{i}q^{b}_{j} = 0 \tag{9}$$

where $q^{b}_{j} = [x_j, y_j]$ and we assume that no external force is acting on the bearing.

The global mass, damping, and stiffness matrices, **M**, **C** and **K** respectively, are obtained by carrying out the so-called assembling process [9], which represents the transition from the individual finite elements to the whole structure. As shown in [9], the equations of motion have the form

$$\mathbf{M}\ddot{q} + \mathbf{C}\dot{q} + \mathbf{K}q = F \tag{10}$$

3. DERIVATION OF IDENTIFICATION FORMULA FOR CASE A: ROTOR PARAMETERS ARE ALL KNOWN

For ease of presentation, assume that the rotor is supported by two bearings at each end of the shaft, divided by n elements, and driven by an unbalance force with spin speed Ω. Then, Eqn (10) takes the following form:

$$\begin{bmatrix} \begin{bmatrix}\mathbf{M}^{s}_{1}\end{bmatrix} & & & \\ & \begin{bmatrix}\mathbf{M}^{s}_{2}\end{bmatrix} & & \\ & & \cdots & \\ & & & \begin{bmatrix}\mathbf{M}^{s}_{n}\end{bmatrix} \end{bmatrix} \ddot{q} + \begin{bmatrix} \begin{bmatrix}\mathbf{M}^{r}_{1}\end{bmatrix} & & & \\ & \begin{bmatrix}\mathbf{M}^{r}_{2}\end{bmatrix} & & \\ & & \cdots & \\ & & & \begin{bmatrix}\mathbf{M}^{r}_{n}\end{bmatrix} \end{bmatrix} \ddot{q}$$

$$+ \begin{bmatrix} \begin{bmatrix}\mathbf{G}^{e}_{1}\end{bmatrix} & & & \\ & \begin{bmatrix}\mathbf{G}^{e}_{2}\end{bmatrix} & & \\ & & \cdots & \\ & & & \begin{bmatrix}\mathbf{G}^{e}_{n}\end{bmatrix} \end{bmatrix} \dot{q} + \begin{bmatrix} \begin{bmatrix}\mathbf{K}^{e}_{1}\end{bmatrix} & & & \\ & \begin{bmatrix}\mathbf{K}^{e}_{2}\end{bmatrix} & & \\ & & \cdots & \\ & & & \begin{bmatrix}\mathbf{K}^{e}_{n}\end{bmatrix} \end{bmatrix} q$$

$$+ \begin{bmatrix} [\mathbf{C}^{b}_{1}\ 0] & & \\ & \cdots & \\ & & [\mathbf{C}^{b}_{2}\ 0] \end{bmatrix} \dot{q} + \begin{bmatrix} [\mathbf{K}^{b}_{1}\ 0] & & \\ & \cdots & \\ & & [\mathbf{K}^{b}_{2}\ 0] \end{bmatrix} q$$

$$+ \begin{bmatrix} 0 & & & \\ & [\mathbf{M}^{d}_{1}] & & \\ & & \cdots & \\ & & & \mathbf{M}^{d}_{D} \\ & & & & [0] \end{bmatrix} \ddot{q} + \begin{bmatrix} 0 & & & \\ & \mathbf{G}^{d}_{1} & & \\ & & \cdots & \\ & & & \mathbf{G}^{d}_{D} \\ & & & & 0 \end{bmatrix} \dot{q}$$

$$= \mathbf{M}^{a}\ddot{q} + \mathbf{C}^{a}\dot{q} + \mathbf{K}^{a}q + \mathbf{C}^{b}\dot{q} + \mathbf{K}^{b}q = F(t) \tag{11}$$

where

$$F(t) = [f_{x1}(t),\ f_{y1}(t),\ T_{\theta y1}(t),\ T_{\theta x1}(t),\ f_{x2}(t),\ f_{y2}(t),\ T_{\theta y2}(t),$$
$$T_{\theta x2}(t), \ldots,\ f_{x(n+1)},\ f_{y(n+1)},\ T_{\theta y(n+1)}(t),\ T_{\theta x(n+1)}\ (t)]^{t}$$
$$= [0,\ 0,\ 0,\ 0,\ f_{x2}(t),\ f_{y2}(t),\ 0,\ 0,$$
$$f_{x3}(t),\ f_{y3}(t),\ 0,\ 0, \ldots, f_{xn},\ f_{yn},\ 0,\ 0,\ 0,\ 0,\ 0,\ 0]^{t}$$

$$\mathbf{M}^{a} = \begin{bmatrix} \begin{bmatrix} \mathbf{M}_1^{s} \end{bmatrix} & & & \\ & \begin{bmatrix} \mathbf{M}_2^{s} \end{bmatrix} & & \\ & & \cdots & \\ & & & \begin{bmatrix} \mathbf{M}_n^{s} \end{bmatrix} \end{bmatrix} + \begin{bmatrix} \begin{bmatrix} \mathbf{M}_1^{r} \end{bmatrix} & & & \\ & \begin{bmatrix} \mathbf{M}_2^{r} \end{bmatrix} & & \\ & & \cdots & \\ & & & \begin{bmatrix} \mathbf{M}_n^{r} \end{bmatrix} \end{bmatrix}$$

$$+ \begin{bmatrix} 0 & & & \\ & \mathbf{M}_1^{d} & & \\ & & \cdots & \\ & & & \mathbf{M}_D^{d} \\ & & & & 0 \end{bmatrix}$$

$$\mathbf{C}^{a} = \begin{bmatrix} \begin{bmatrix} \mathbf{G}_1^{e} \end{bmatrix} & & & \\ & \begin{bmatrix} \mathbf{G}_2^{e} \end{bmatrix} & & \\ & & \cdots & \\ & & & \begin{bmatrix} \mathbf{G}_n^{e} \end{bmatrix} \end{bmatrix} + \begin{bmatrix} 0 & & & \\ & \mathbf{G}_1^{d} & & \\ & & \cdots & \\ & & & \mathbf{G}_D^{d} \\ & & & & 0 \end{bmatrix},$$

$$\mathbf{K}^{a} = \begin{bmatrix} \begin{bmatrix} \mathbf{K}_1^{e} \end{bmatrix} & & & \\ & \begin{bmatrix} \mathbf{K}_2^{e} \end{bmatrix} & & \\ & & \cdots & \\ & & & \begin{bmatrix} \mathbf{K}_n^{e} \end{bmatrix} \end{bmatrix}$$

$$\mathbf{C}^{b} = \begin{bmatrix} [\mathbf{C}_1^{b}\ 0] & & \\ & \cdots & \\ & & [\mathbf{C}_2^{b}\ 0] \end{bmatrix} \quad \mathbf{K}^{b} = \begin{bmatrix} [\mathbf{K}_1^{b}\ 0] & & \\ & \cdots & \\ & & [\mathbf{K}_2^{b}\ 0] \end{bmatrix}$$

Here it is assumed that there is no external force acting on the bearings and no bending moment on the system. Consider the case when the rotor parameters, including shaft and disks, are all known. $\mathbf{M}^{a}$, $\mathbf{C}^{a}$, and $\mathbf{K}^{a}$ are $(4n+4)\times(4n+4)$ known matrices, and $\mathbf{C}_i^{b}$, $\mathbf{K}_i^{b}$ $(i = 1, 2)$, 2×2 unknown submatrices to be estimated. The responses about the deflection angle for this case can be replaced by deflections as will be shown in the following.

We arrange q in the form $[z^{t}, \theta^{t}]^{t}$, $\mathbf{F}$ in $[f^{t}, T^{t}]^{t}$ in Eqn (11), where $z = [x_1, x_2, \ldots, x_{n+1}, y_1, y_2, \ldots, y_{n+1}]^{t}$, $\theta = [l\theta_{y1}, l\theta_{y2}, \ldots, l\theta_{y(n+1)}, l\theta_{x1}, l\theta_{x2}, \ldots, l\theta_{x(n+1)}]^{t}$, $f = f_{x1}, f_{x2}, \ldots, f_{x(n+1)}$,

$f_{y1}, f_{y2}, \ldots, f_{y(n+1)}]^t$, and $\mathbf{T} = [T_{x1}, T_{x2}, \ldots, T_{x(n+1)}, T_{y1}, T_{y2}, \ldots, T_{y(n+1)}]^t = 0$. Equation (11) can then be rewritten as

$$\begin{bmatrix} m_{zz} & m_{z\theta} \\ m_{\theta z} & m_{\theta\theta} \end{bmatrix} \begin{bmatrix} \ddot{z} \\ \ddot{\theta} \end{bmatrix} + \begin{bmatrix} c_{zz} & c_{z\theta} \\ c_{\theta z} & c_{\theta\theta} \end{bmatrix} \begin{bmatrix} \dot{z} \\ \dot{\theta} \end{bmatrix} + \begin{bmatrix} k_{zz} & k_{z\theta} \\ k_{\theta z} & k_{\theta\theta} \end{bmatrix} \begin{bmatrix} z \\ \theta \end{bmatrix}$$

$$+ \begin{bmatrix} c^b_{zz} & 0 \\ 0 & 0 \end{bmatrix} \begin{bmatrix} \dot{z} \\ \dot{\theta} \end{bmatrix} + \begin{bmatrix} k^b_{zz} & 0 \\ 0 & 0 \end{bmatrix} \begin{bmatrix} z \\ \theta \end{bmatrix} = \begin{bmatrix} f \\ 0 \end{bmatrix} \tag{12}$$

where c^b_{zz} and k^b_{zz}, the damping and stiffness matrices of the bearings, have the following form:

$$c^b_{zz} = \begin{bmatrix} c^b_{xx1} & \cdots & 0 & c^b_{xy1} & \cdots & 0 \\ & \cdots & & & \cdots & \\ 0 & \cdots & c^b_{xx2} & 0 & \cdots & c^b_{xy2} \\ c^b_{yx1} & \cdots & 0 & c^b_{yy1} & \cdots & 0 \\ & \cdots & & & \cdots & \\ 0 & \cdots & c^b_{yx2} & 0 & \cdots & c^b_{yy2} \end{bmatrix} (2n+2)\times(2n+2)$$

$$k^b_{zz} = \begin{bmatrix} k^b_{xx1} & \cdots & 0 & k^b_{xy1} & \cdots & 0 \\ & \cdots & & & \cdots & \\ 0 & \cdots & k^b_{xx2} & 0 & \cdots & k^b_{xy2} \\ k^b_{yx1} & \cdots & 0 & k^b_{yy1} & \cdots & 0 \\ & \cdots & & & \cdots & \\ 0 & \cdots & k^b_{yx2} & 0 & \cdots & k^b_{yy2} \end{bmatrix} (2n+2)\times(2n+2) \tag{13}$$

From Eqn (12), the following equations can be obtained:

$$m_{zz}\ddot{z} + c_{zz}\dot{z} + k_{zz}z + m_{z\theta}\ddot{\theta} + c_{z\theta}\dot{\theta} + k_{z\theta}\theta + c^b_{zz}\dot{z} + k^b_{zz}z = f \tag{14}$$

$$m_{\theta z}\ddot{z} + c_{\theta z}\dot{z} + k_{\theta z}z + m_{\theta\theta}\ddot{\theta} + c_{\theta\theta}\dot{\theta} + k_{\theta\theta}\theta = 0 \tag{15}$$

Applying a Fourier transform to the vectors z and θ, one obtains

$$z(t) = z_c \cos\Omega t + z_s \sin\Omega t \tag{16}$$

$$\theta(t) = \theta_c \cos\Omega t + \theta_s \cos\Omega t \tag{17}$$

where z_c, z_s, θ_c, and θ_s are $(2n+2)\times 1$ constant vectors.
By substituting Eqns (16–17) into Eqn (15), the following relationship can be obtained:

$$\theta_c = \mathbf{E}z_c + \mathbf{F}z_s \tag{18}$$

$$\theta_s = \mathbf{G}z_c + \mathbf{H}z_s \tag{19}$$

We can substitute Eqns (16–19) into Eqn (14), extract the first and $(n+2)$'th rows of Eqn (14), and take the transpose on both sides to obtain the following equation:

$$w^t_c \cos\Omega t + w^t_s \sin\Omega t)_{1\times 4}\, P_{4\times 2} = (f^t_{ac}\cos\Omega t + f^t_{as}\sin\Omega t)_{1\times 2} \tag{20}$$

where $\mathbf{P}^t = [\mathbf{C}^b_1\ \mathbf{K}^b_1]$, $w(t) = [\dot{x}_1(t), \dot{y}_1(t), x_1(t), y_1(t)]^t = (w_c\cos\Omega t + w_s\sin\Omega t)$, and w_c, w_s, f_{ac}, and f_{as} are constant matrices and functions of z_c and z_s. The matrices **E**, **F**, **G**, **H**, w_c, w_s, f_{ac}, and f_{as} are derived as shown in Appendix B.

Since the estimates of the parameter matrix **P**, denoted by $\hat{\mathbf{P}}$, will be inexact because of random disturbance and measurement errors, an error vector function $e(t)$ can be defined as follows:

$$e^t(t) = f^t_{ac}\cos\Omega t + f^t_{as}\sin\Omega t - [w^t_c\cos\Omega t + w^t_s\sin\Omega t]\,\hat{\mathbf{P}} \tag{21}$$

We can now define a cost function, C, as the integral over a cycle 0 to $2\pi/\Omega$ of the error squared, i.e.

$$C = \int_0^{2\pi/\Omega} e^t(t)\, e(t)\, dt = \int_0^{2\pi/\Omega} \sum_{i=1}^{2} e_i^2(t)\, dt \tag{22}$$

Now we will choose $\hat{\mathbf{P}}$ in such a way that the cost function C is minimized. Differentiate C with respect to $\hat{\mathbf{P}}$ and equate the result to zero to determine the condition that minimizes C. Thus

$$\partial C/\partial \hat{P} = \int_0^{2\pi/\Omega} -2\,[w_s^t \cos\Omega t + w_s^t \sin\Omega t]^t\, [f_{ac}^t \cos\Omega t] + f_{as}^t \sin\Omega t]$$

$$+ 2\{w_c^t \cos\Omega t + w_s^t \sin\Omega t]^t\, [\, w_c^t \cos\Omega t + w_s^t \sin\Omega t]\hat{\mathbf{P}}\, dt = 0 \tag{23}$$

This yields

$$\mathbf{A}\hat{\mathbf{P}} = \mathbf{B} \tag{24}$$

where

$$\mathbf{A} = \int_0^{2\pi/\Omega} [w_c \cos\Omega t + w_s \sin\Omega t]\, [w_c^t \cos\Omega t + w_s^t \sin\Omega t]\, dt$$

$$\mathbf{B} = \int_0^{2\pi/\Omega} [w_c \cos\Omega t + w_s \sin\Omega t]\, [f_{ac}^t \cos\Omega t + f_{as}^t \sin\Omega t]\, dt \tag{25}$$

and $\mathbf{A}$ and $\mathbf{B}$ are 4×4 and 4×2 matrices. Equation (25) involves the integration of a product of two sinusoidally varying signals. To solve for matrices $\mathbf{A}$ and $\mathbf{B}$ the following relationships were used:

$$\int_0^{2\pi/\Omega} \sin^2 \Omega t\, dt = \int_0^{2\pi/\Omega} \cos^2 \Omega t\, dt = \pi/\Omega \tag{26}$$

$$\int_0^{2\pi/\Omega} \sin\Omega t \cos\Omega t\, dt = 0 \tag{27}$$

Then $\mathbf{A}$ and $\mathbf{B}$ can be obtained as

$$\mathbf{A} = \pi/\Omega\, (w_c w_c^t + w_s w_s^t) \tag{28}$$

$$\mathbf{B} = \pi/\Omega\, (w_c f_{ac}^t + w_s f_{as}^t) \tag{29}$$

and they are independent of time. From Eqns (24), (28) and (29), $\hat{\mathbf{P}}$ can be solved as

$$\hat{\mathbf{P}} = \mathbf{A}^{-1}\mathbf{B} \tag{30}$$

This result is called the least-squares estimator (LSE) of $\hat{\mathbf{P}}$. Equation (24) is referred to as the normal equation and C is called the residual in the statistics literature.

Equation (30) will yield the required coefficient estimates only if $\mathbf{A}$ is non-singular, and it is necessary to establish the conditions under which this is satisfied. It can be shown that if two independent sinusoidal signals exist at the same frequency Ω, then any other signal can be expressed as a linear combination of them. Hence if the number of variables, n, in vector w is greater than 2, then $(n-2)$ linear relationships exist between the n variables. This entails that the rank of $\mathbf{A}$ is 2; $\mathbf{A}$ is thus singular and no unique solution for $\mathbf{P}$ is possible. To overcome this problem, we use two different spin speeds to estimate the eight bearing coefficients. From engineering considerations, although different spin speeds result in different coefficients of the bearings, the coefficients of the bearings can be assumed to vary smoothly and only slightly when the spin speed changes slightly. Thus, the bearing characteristics can be assumed to be equal at two close spin speeds. Equation (24) can be rewritten as

$$\mathbf{A}_i\hat{\mathbf{P}}_i = \mathbf{B}_i \quad (i = 1, 2) \tag{31}$$

where the index i denotes that the system was driven at spin speed Ω_i.

Since the difference between $\hat{\mathbf{P}}_1$ and $\hat{\mathbf{P}}_2$ is small, they can be set to be $\hat{\mathbf{P}}$ and the following equation can be derived.

$$(\mathbf{A}_1 + \mathbf{A}_2)\, \hat{\mathbf{P}} = (\mathbf{B}_1 + \mathbf{B}_2) \tag{32}$$

The solution of Eqn (32) can be obtained by the least-squares method.

$$\mathbf{P} = (\mathbf{A}_1 + \mathbf{A}_2)^{-1} (\mathbf{B}_1 + \mathbf{B}_2) \tag{33}$$

A block diagram of the estimation process proposed in this section is shown in Fig. 3. The $(n+1)$th and $(2n+2)$th rows of Eqn (14) can be extracted by a similar procedure to estimate the parameters of the second bearing.

4. DERIVATION OF IDENTIFICATION FORMULA FOR CASE B: ROTOR PARAMETERS IN THE VICINITY OF THE SUPPORTS KNOWN

In this case the characteristics of the bearing are to be estimated when the rotor parameters in the vicinity of the supports are known. For example, the characteristics of bearing 1 are to be estimated when $(\mathbf{M}_1^s)^*$, $(\mathbf{M}_1^r)^*$, $(\mathbf{C}_1^e)^*$ and $(\mathbf{K}_1^e)^*$ are known. We extract the first two rows of Eqn (11) and reorganize them in the following form:

$$\mathbf{C}_1^b \begin{bmatrix} \dot{x}_1 \\ \dot{y}_1 \end{bmatrix} + \mathbf{K}_1^b \begin{bmatrix} x_1 \\ y_1 \end{bmatrix} = [(\mathbf{M}_1^s)^* + (\mathbf{M}_1^r)^*] \ddot{q}_1^e(t) - (\mathbf{C}_1^e)^* \dot{q}_1^e(t) - (\mathbf{K}_1^e)^* q_1^e(t) \equiv f_a \tag{34}$$

From Eqn (34), f_a can be regarded as an artificial force vector, and it can be measured since the characteristics of the first segments $(\mathbf{M}_1^s)^*$, $(\mathbf{M}_1^r)^*$, $(\mathbf{C}_1^e)^*$, and $(\mathbf{K}_1^e)^*$ are specified. Introduce the 2×4 matrix

$$\mathbf{P}^t = [\mathbf{C}_1^b \; \mathbf{K}_1^b] \tag{35}$$

and the 4×1 vector

$$w(t) = [\dot{x}_1(t), \dot{y}_1(t), x_1(t), y_1(t)]^t \tag{36}$$

In terms of this notation, Eqn (34) can be rewritten in the form

$$\mathbf{P}^t w(t) = f_a(t) \tag{37}$$

The transposition of each side of Eqn (37) yields

$$\mathbf{w}^t(t)\mathbf{P} = f_a^t(t) \tag{38}$$

Since the response of the rotor contains only a synchronous frequency component, by a process similar to that in Case A, Eqn (38) can be written as

$$(w_c^t \cos \Omega t + w_s^t \sin \Omega t)\, \hat{P} = (f_{ac}^t \cos \Omega t + f_{as}^t \sin \Omega \tau t) \tag{39}$$

where

$$w(t) = (w_c \cos \Omega t + w_s \sin \Omega t)$$

and

$$f_a(t) = f_{ac} \cos \Omega t + f_{as} \sin \Omega \tau t$$

The error vector $e(t)$ becomes

$$e^t(t) = (f_{ac}^t \cos \Omega t + f_{as}^t \sin \Omega \tau t) - (w_c^t \cos \Omega t + w_s^t \sin \Omega t)\hat{P} \tag{40}$$

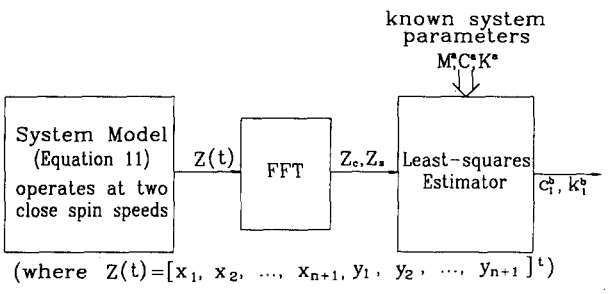

Fig. 3. Block diagram of the estimation process (Case A).

and the cost function has the form

$$C = \int_0^{2\pi/\Omega} e^{t}(t)\, e(t)\, dt = \int_0^{2\pi/\Omega} \sum_{i=1}^{2} e_i^2(t)\, dt \tag{41}$$

Differentiating C with respect to $\hat{\mathbf{P}}$ and equating the result to zero, one obtains

$$\mathbf{A}\hat{\mathbf{P}} = \mathbf{B} \tag{42}$$

here $\mathbf{A} = \pi/\Omega\ (w_c w_c^t + w_s w_s^t)$, $\mathbf{B} = \pi/\Omega(w_c f_{ac}^t + w_s f_{as}^t)$, and $\mathbf{A}$ and $\mathbf{B}$ are 4×4 and 4×2 matrices.

If a single spin speed is used, the rank of $\mathbf{A}$ is 2 and singular. By the same assumption as in Case A, we can use two spin speeds to estimate the value of the coefficients of the bearings. A block diagram of the estimation process is shown in Fig. 4.

5. DERIVATION OF IDENTIFICATION FORMULA FOR CASE C: ROTOR PARAMETERS ARE UNKNOWN EXCEPT FOR THE MASS OF ELEMENTS IN THE VICINITY OF THE SUPPORTS

When the rotor parameters are unknown except for the mass of elements in the vicinity of the supports (m_1^s), the characteristics of bearing 1 are to be estimated. Referring to Eqn (7), we can rewrite Eqn (34) as

$$[\mathbf{C}_1^b, \mathbf{O}_{2\times6}]_{2\times8}\, \dot{q}_1^e + [\mathbf{K}_1^b, \mathbf{O}_{2\times6}]_{2\times8}\, q_1^e + m_1^r\, \mathbf{L}_r^*\, \ddot{q}_1^e + c_1^e \mathbf{L}_c^*\, \dot{q}_1^e + k_1^e \mathbf{L}_k^*\, q_1^e = -m_1^s \mathbf{L}_s^*\, \ddot{q}_1^e \tag{43}$$

From Eqn (43), we can set

$$P_1 = c_{xx1}^b, \quad P_2 = c_{xy1}^b, \quad P_3 = c_{y\times1}^b, \quad P_4 = c_{yy1}^b$$
$$P_5 = k_{xx1}^b, \quad P_6 = k_{xy1}^b, \quad P_7 = k_{y\times1}^b, \quad P_8 = k_{yy1}^b$$
$$P_9 = m_1^r, \quad P_{10} = c_1^e, \quad P_{11} = k_1^e$$

Then Eqn (43) can be written in the following form

$$\mathbf{D}(\mathbf{P})\, \mathbf{W}(t) = f_a(t) \tag{44}$$

where

$$\mathbf{D}(\mathbf{P}) = [\mathbf{D}_1, \mathbf{D}_2, \ldots, \mathbf{D}_5]$$
$$\mathbf{D}_1 = [\mathbf{C}_1^b, \mathbf{O}_{2\times6}]_{2\times8} \quad \mathbf{D}_2 = [\mathbf{K}_1^b, \mathbf{O}_{2\times6}]_{2\times8}$$
$$\mathbf{D}_3 = m_1^r\, \mathbf{L}_r^* \quad \mathbf{D}_4 = c_1^e\, \mathbf{L}_c^*$$
$$\mathbf{D}_5 = k_1^e\, \mathbf{L}_k^*$$
$$\mathbf{W}(t) = [(\dot{q}_1^e)^t, (q_1^e)^t, (\ddot{q}_1^e)^t, (\dot{q}_1^e)^t, (\dot{q}_1^e)^t]^t$$
$$f_a(t) = -m_1^s\, \mathbf{L}_s^*\, \ddot{q}_1^e$$
$$\mathbf{P} = [P_1, P_2, \ldots, P_{11}]^t$$

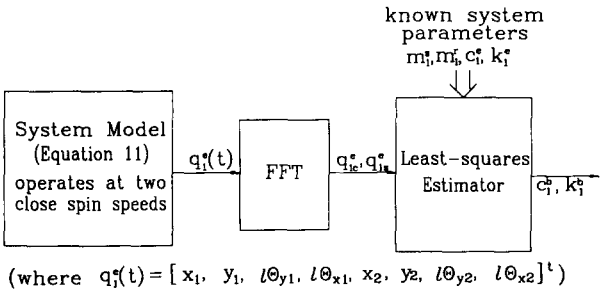

Fig. 4. Block diagram of the estimation process (Case B).

The matrix **D** can be written as

$$\mathbf{D}(\mathbf{P}) = \sum_{n=1}^{11} (\partial \mathbf{D}/\partial P_n) P_n \tag{45}$$

and Eqn (44) can be expressed explicitly in the form of parameters as follows:

$$\sum_{n=1}^{11} [(\partial \mathbf{D}/\partial P_n)\, \mathbf{W}(t)]\, P_n = f_a(t) \tag{46}$$

The main feature of Eqn (46) is that the system parameters are extracted from the matrices, which makes the identification feasible.

Let $\mathbf{a}_n = (\partial \mathbf{D}/\partial P_n)\mathbf{W}(t)$ be a 2×1 vector obtained by multiplying displacement, velocity, and acceleration by the corresponding matrices. The details of $\mathbf{a}_n$ are shown in Appendix C. Rearrange Eqn (46) and introduce the equation

$$\mathbf{a}(t)\mathbf{P} = f_a(t) \tag{47}$$

where

$$\mathbf{a}(t) = [a_1, a_2, \ldots, a_{11}]$$

$\mathbf{a}$ is a 2×11 known matrix, f_a is a 2×1 known vector, and $\mathbf{P}$ is a 11×1 unknown vector to be estimated if the mass of the first element (i.e. m_1^s) is known. There are two equations and 11 unknowns to be solved. The steady state of the rotor will contain only a synchronous frequency component, hence by applying a Fourier transform to the measured displacement $\mathbf{q}_1^c(t)$, one obtains:

$$q_1^c(t) = q_{1c}^c \cos \Omega t + q_{1s}^c \sin \Omega t \tag{48}$$

where the constant vectors $\mathbf{q}_{1c}^c$ and $\mathbf{q}_{1s}^c$ are generated by the Fourier transform. Thus:

$$\dot{q}_1^c = \Omega(q_{1s}^c \cos \Omega t - q_{1c}^c \sin \Omega t) \tag{49}$$

$$\ddot{q}_1^c = -\Omega^2(q_{1c}^c \cos \Omega t + q_{1s}^c \sin \Omega t) \tag{50}$$

Substituting Eqn (48–50) into Eqn (47) and rearranging the sine and cosine terms, one can obtain:

$$[\mathbf{a}_c \cos \Omega t + \mathbf{a}_s \sin\ \Omega t)\mathbf{P} = f_{ac} \cos \Omega t + f_{as} \sin \Omega t \tag{51}$$

where $\mathbf{a}_c$ and $\mathbf{a}_s$ are 2×11 constant matrices and f_{ac} and f_{as} 2×1 constant vectors. Similar to Case A, we can obtain the normal equation as follows:

$$\mathbf{A}\hat{\mathbf{P}} = \mathbf{B} \tag{52}$$

where

$$\mathbf{A} = \pi/\Omega(\mathbf{a}_c^t \mathbf{a}_c + \mathbf{a}_s^t \mathbf{a}_s) \tag{53}$$

$$\mathbf{B} = \pi/\Omega(\mathbf{a}_c^t f_{ac} + \mathbf{a}_s^t f_{as}) \tag{54}$$

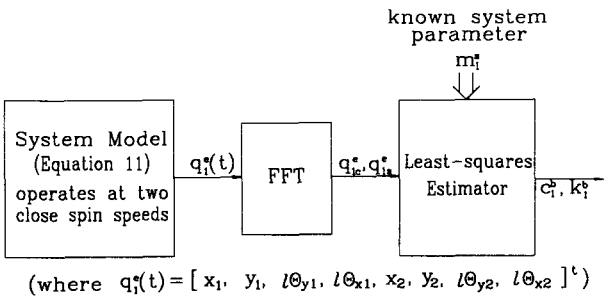

Fig. 5. Block diagram of the estimation process (Case C).

and they are independent of time. The rank of 11×11 matrix $\mathbf{A}$ is 4 when a single spin speed is used. Although the rank $\mathbf{A}$ can be increased to 8 by using two different spin speeds, it is still singular. The dimension of $\mathbf{a}_i$ must be increased and, therefore, the first four rows of Eqn (11) must be extracted. To increase the dimension of $\mathbf{a}_i$, we replace the 2×8 matrices $\mathbf{L}_s^*$, $\mathbf{L}_r^*$, $\mathbf{L}_c^*$, and $\mathbf{L}_k^*$ by 4×8 matrices $\mathbf{L}_s^\#$, $\mathbf{L}_r^\#$, $\mathbf{L}_c^\#$, and $\mathbf{L}_k^\#$. Then $\mathbf{a}_i$ is modified as shown in Appendix D, and Eqn (52) can be rewritten as

$$\mathbf{A}_i \hat{\mathbf{P}}_i = \mathbf{B}_i \quad (i = 1, 2)$$

where the index i denotes that the system was driven at spin speed Ω_i. Assume the difference between $\hat{\mathbf{P}}_1$ and $\hat{\mathbf{P}}_2$ is small and set them to be $\hat{\mathbf{P}}$. The parameter vector $\mathbf{P}$ can be estimated by

$$\mathbf{P} = (\mathbf{A}_1 + \mathbf{A}_2)^{-1}(\mathbf{B}_1 + \mathbf{B}_2)$$

6. DIGITAL SIMULATION AND DISCUSSION

A flexible rotor-bearing system with two bearings mounted at the ends of the shaft is used here as a numerical example. The system is modelled by the finite-element method with ten elements (see Fig. 6). The Young's modulus E and density ρ of the shaft are $2 \times 10^{11}\ \mathrm{N m^{-2}}$ and $7750\ \mathrm{kg m^{-3}}$. The diametric and polar mass moment inertia of the two disks are 0.292 and $0.584\ \mathrm{kg \cdot m^2}$. The shaft and disks are symmetric and the unbalance mass for disk 1 is at a distance of 2 cm from the geometric center. In the following three cases, the measurement responses are taken at spin speeds of 95 and 105 $\mathrm{rad\ s^{-1}}$, respectively. Here we assume that the characteristics of the bearings are the same at these two close spin speeds. The responses are contaminated with additive noise of different levels drawn from independent sequences of normally distributed random numbers to examine the noise rejection properties of the proposed methods. The Noise to signal ratio (NSR) is defined as

$$\mathrm{NSR} = \mathrm{STD}[n(t)]/\mathrm{STD}[s(t)] \tag{55}$$

where $n(t)$ is noise, $s(t)$ is signal, and the operator $\mathrm{STD}[\cdot]$ is standard deviation. Simulation results for three cases using different parameter estimators are shown in Tables 1–3.

In Case A, we assume that the characteristics of the shaft and disks are known. Using the method described in Section 3, we can estimate the parameters of bearing 1 (and bearing 2) by taking the deflection responses of all nodes (x_i, y_i; $i = 1, 2, \ldots, 11$). The results are shown in Table 1. When the characteristics of segment 1 (i.e. m_1^s, m_1^r, c_1^e, and k_1^e) are known *a priori* for Case B, the method in Section 4 is adopted to estimate the parameters of bearing 1 by taking the measurement responses (including deflections and deflection angles) of nodes 1 and 2 (i.e. x_1, y_1, θy_1, θ_{x1}, x_2, y_2, θ_{y2}, θ_{x2}). The results are shown in Table 2. In Case C, only the information about the mass of segment 1 (m_1^s) is given. Using the method described

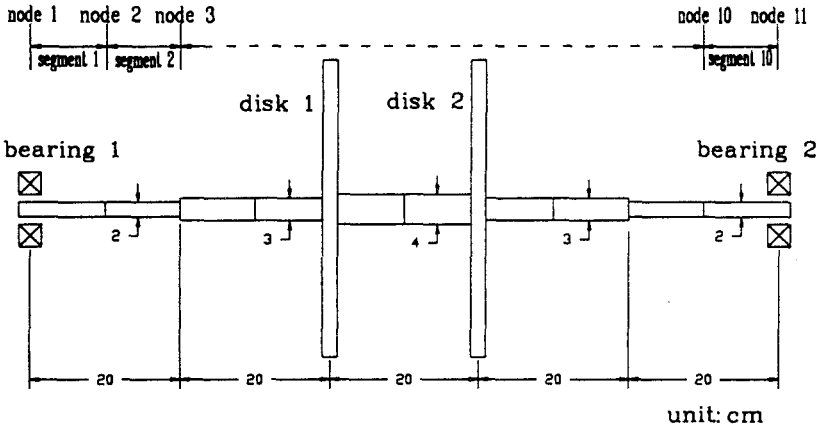

Fig. 6. A simulated rotor-bearing system.

Table 1. Estimation results from simulation data for Case A

	$k^b_{xx}(10^6\,\mathrm{Nm^{-1}})$	$k^b_{xy}(10^5\,\mathrm{Nm^{-1}})$	$k^b_{yx}(10^5\,\mathrm{Nm^{-1}})$	$k^b_{yy}(10^6\,\mathrm{Nm^{-1}})$
True value	2.000	1.000	1.000	2.000
NSR 0%	1.999	1.000	1.000	1.999
1.0%	1.999	1.000	0.922	1.999
5.0%	1.999	1.002	0.995	1.999
20.0%	2.000	1.010	0.982	1.997
40.0%	2.000	1.020	0.964	1.994
(average of 25 signals)				
NSR 1.0%	1.999	1.000	1.000	1.999
5.0%	2.000	1.002	0.999	1.999
20.0%	2.000	1.007	0.998	1.999
40.0%	2.001	1.014	0.993	1.997
	$c^b_{xx}(10^2\,\mathrm{Nsm^{-1}})$	$c^b_{xy}(10^2\,\mathrm{Nsm^{-1}})$	$c^b_{yx}(10^2\,\mathrm{Nsm^{-1}})$	$c^b_{yy}(10^2\,\mathrm{Nm^{-1}})$
True value	6.000	4.000	4.000	6.000
NSR 0%	6.000	3.989	4.007	5.996
1.0%	5.994	3.977	4.005	5.990
5.0%	5.960	3.929	3.995	5.696
20.0%	5.836	3.752	3.977	5.889
40.0%	5.677	3.524	3.949	5.783
(average of 25 signals)				
NSR 0.1%	6.003	3.989	4.007	5.996
1.0%	6.005	3.992	4.006	5.998
5.0%	6.017	4.002	4.006	6.006
20.0%	6.061	4.041	4.004	6.037
40.0%	6.119	4.095	4.002	6.078

Table 2. Estimation results from simulation data for Case B

	$k^b_{xx}(10^6\,\mathrm{Nm^{-1}})$	$k^b_{xy}(10^5\,\mathrm{Nm^{-1}})$	$k^b_{yx}(10^5\,\mathrm{Nm^{-1}})$	$k^b_{yy}(10^6\,\mathrm{Nm^{-1}})$
True value	2.000	1.000	1.000	2.000
NSR 0%	2.000	1.000	1.000	2.000
0.1%	2.000	0.999	0.910	2.007
1.0%	2.002	0.999	0.098	2.079
5.0%	2.000	0.995	− 35.2	2.396
(average of 25 signals)				
NSR 0.1%	2.000	0.999	0.931	2.000
1.0%	2.000	0.999	0.981	2.000
5.0%	2.000	0.997	− 24.4	2.020
	$c^b_{xx}(10^2\,\mathrm{Nsm^{-1}})$	$c^b_{xy}(10^2\,\mathrm{Nsm^{-1}})$	$c^b_{yx}(10^2\,\mathrm{Nsm^{-1}})$	$c^b_{yy}(10^2\,\mathrm{Nsm^{-1}})$
True value	6.000	4.000	4.000	6.000
NSR 0%	6.000	4.000	4.000	6.000
0.1%	5.999	3.999	4.799	6.834
1.0%	5.931	3.998	11.99	14.34
5.0%	5.956	3.991	43.81	47.81
(average of 25 signals)				
NSR 0.1%	6.000	3.999	4.115	6.177
1.0%	6.002	3.999	5.157	7.767
5.0%	6.010	3.990	9.820	14.85

in Section 5, we can estimate the parameters of bearing 1 by measuring the responses of nodes 1 and 2 (i.e. x_1, y_1, θ_{y1}, θ_{x1}, x_2, y_2, θ_{y2}, θ_{x2}) as in Case B; the results are shown in Table 3.

The results in Table 1 show that the estimation in this case is less sensitive than those in Tables 2 and 3. A high noise to signal ratio (NSR) has little effect on the coefficient estimates even when signal averaging is not used. In Table 2, the estimates are refined effectively when signal averaging is used. From Table 3, we find that the sensitivity to noise is high even when signal averaging is used.

In our estimates for all cases, the artificial force terms f_a, shown in Eqns (20), (34) and (44), are the combinations of measurements. This means that the NSRs of the artificial forces are no longer equal to the NSRs of the measurements. To further investigate this phenomenon, let us derive the NSR of f_a as a function of the NSR of the measurements for Case B. Neglect the velocity term in Eqn (34), which is small in order of magnitude compared with the other terms (see Appendix E), and define measurement vector $\mathbf{q}_1^e$ as

$$q_1^e = q_{1o}^e + q_{1n}^e = q_{1c}^e \cos \Omega t + \mathbf{q}_{1s}^e \sin \Omega t + q_{1n}^e$$

where q_{1o}^e is the true value of measurements and q_{1n}^e is the measurement noise. Then $\mathbf{f}_a(t)$ can be written as

$$\begin{aligned} f_a(t) = \begin{bmatrix} f_1(t) \\ f_2(t) \end{bmatrix} &= -[(\mathbf{M}_1^s)^* + (\mathbf{M}_1^r)^*]\ddot{q}_1^e - (\mathbf{K}_1^e)^* q_1^e \\ &= \{\Omega^2[(\mathbf{M}_1^s)^* + (\mathbf{M}_1^r)^*] - (\mathbf{K}_1^e)^*\} q_1^e \\ &= \mathbf{C}(q_{1c}^e \cos \Omega t + q_{1s}^e \sin \Omega t + q_{1n}^e) \end{aligned}$$

or

$$\begin{aligned} f_i(t) &= \sum_{j=1}^{8} C_{ij}[(q_{1c}^e)_j \cos \Omega t + (q_{1s})_j \sin \Omega t + (q_{1n}^e)_j] \\ &= f_{io}(t) + f_{in}(t) \quad i = 1, 2 \end{aligned} \tag{56}$$

where

$$\mathbf{C} = \Omega^2((\mathbf{M}_1^s)^* + (\mathbf{M}_1^r)^*] - (\mathbf{K}_1^e)^*$$

$$f_{io}(t) = \sum_{j=1}^{8} C_{ij}[(q_{1c}^e)_j \cos \Omega t + (q_{1s}^e)_j \sin \Omega t]$$

$$f_{in}(t) = \sum_{j=1}^{8} C_{ij}(q_{1n}^e)_j$$

Table 3. Estimation results from simulation data for Case C

	$k_{xx}^b(10^6\,\mathrm{Nm}^{-1})$	$k_{xy}^b(10^5\,\mathrm{Nm}^{-1})$	$k_{yx}^b(10^5\,\mathrm{Nm}^{-1})$	$k_{yy}^b(10^6\,\mathrm{Nm}^{-1})$
True value	2.000	1.000	1.000	2.000
NSR 0%	2.002	1.001	1.001	2.001
0.1%	− 0.453	0.842	0.369	− 0.52
(average of 25 signals)				
NSR 0.1%	− 0.039	0.086	0.057	− 0.04
	$c_{xx}^b(10^2\,\mathrm{Nsm}^{-1})$	$c_{xy}^b(10^2\,\mathrm{Nsm}^{-1})$	$c_{yx}^b(10^2\,\mathrm{Nsm}^{-1})$	$c_{yy}^b(10^2\,\mathrm{Nsm}^{-1})$
True value	6.000	4.000	4.000	6.000
NSR 0%	6.005	3.995	4.015	6.007
0.1%	1.413	7.815	− 8.831	− 0.756
(average of 25 signals)				
NSR 0.1%	1.409	7.710	− 8.66	− 0.697

$\mathbf{C}$ is a 2×8 coefficient matrix, $f_{io}(t)$ and $f_{in}(t)$ are the true value and measurement noise of artificial force, C_{ij} is the (i, j)th entry of matrix $\mathbf{C}$, and $(q^e_{1c})_j$, $(q^e_{1s})_j$, and $(q^e_{1n})_j$ are the jth entry of vector $\mathbf{q}^e_{1c}$, $\mathbf{q}^e_{1s}$, and $\mathbf{q}^e_{1n}$, respectively. Assume each measurement has the same noise to signal ratio, i.e.

$$\begin{aligned}\text{NSR}_i &= \text{STD}[\mathbf{q}^e_{1n})_i]/\text{STD}[(\mathbf{q}^e_{1o})_i] \\ &= \text{SQRT}[2(V_i^2)/((\mathbf{q}^e_{1c})_i^2 + (\mathbf{q}^e_{1s})_i^2))] = r \quad i = 1, 2, \ldots, 8\end{aligned}$$

where V_i^2 is the variance of $(\mathbf{q}^e_{1n})_i^2$ and the operator SQRT $[\cdot]$ represents square root. The NSR of the artificial force f_i becomes

$$\begin{aligned}\text{NSR of } f_i &= \text{STD}[f_{in}]/\text{STD}[f_{io}] \\ &= \text{STD}\left[\sum_{j=1}^{8} C_{ij}(\mathbf{q}^e_{1n})_j\right] \Big/ \text{STD}\left[\sum_{j=1}^{8} C_{ij}((\mathbf{q}^e_{1c})_j \cos \Omega t + (\mathbf{q}^e_{1s})_j \sin \Omega t)\right] \\ &= \text{SQRT}\left[\left(2\sum_{j=1}^{8} C_{ij}^2 V_j^2\right) \Big/ \left(\left(\sum_{j=1}^{8} C_{ij}(\mathbf{q}^e_{1c})_j\right)^2 + \left(\sum_{j=1}^{8} C_{ij}(\mathbf{q}^e_{1s})_j\right)^2\right)\right] \\ &= \text{SQRT}\left[\left(2\sum_{j=1}^{8} C_{ij}^2 V_j^2\right) \Big/ \left\{\sum_{j=1}^{8} C^2{}_{ij}((\mathbf{q}^e_{1c})_i^2 + (\mathbf{q}^e_{1s})_i^2)\right.\right. \\ &\quad \left.\left. + 2\sum_{\substack{j,k=1 \\ j \neq k}}^{8} (C_{ij}(\mathbf{q}^e_{1c})_j C_{ik}(\mathbf{q}^e_{1c})_k) + (C_{ij}(\mathbf{q}^e_{1s})_j C_{ik}(\mathbf{q}^e_{1s})_k)\right\}\right] \qquad (57)\end{aligned}$$

where we assume that the noise terms $(q^e_{1n})_i$, $i = 1, 2, \ldots, 8$, are independent of each other.

From Eqn (57) we find that, unless the last summation term in the denominator

$$2\sum_{\substack{j,k=1 \\ j \neq k}}^{8} (C_{ij}(\mathbf{q}^e_{1c})_j C_{ik}(\mathbf{q}^e_{ic})_k) + (C_{ij}(\mathbf{q}^e_{1s})_j C_{ik}(\mathbf{q}^e_{1s})_k)$$

vanishes, the NSR of f_i, $i = 1, 2$ never equals r. When this term is negative, the NSR of f_i is larger than any individual measurement; otherwise, the NSR of f_i is smaller.

The NSR of f_a for Case C can be derived by a similar procedure. But for Case A, f_a is function of the deflections at all nodes (x_i, y_i). It is difficult to represent the NSR of f_a in terms of the NSR of each measurement in a compact form. However, in most cases the NSR of $\mathbf{f}_i$ is not equal to that of each measurement in our estimators.

For Cases A and B, the first column of the parameter matrix $\mathbf{P}$ is determined by f_1 and the other column is determined by f_2 [see Eqns (20) and (38)]. For Case A, we find that the NSRs of f_1 and f_2 are both smaller than those of the measurements, which makes the estimates almost totally insensitive to noise when the estimator is used. But for Case B, the NSR of f_2 is larger than the NSR of f_1 and this makes the estimation of k_{yx}, k_{yy}, c_{yx} and c_{yy} more sensitive to noise than that of k_{xx}, k_{xy}, c_{xx} and c_{xy}, as shown in Table 2. To estimate more accurate parameters in this situation, we must reduce the effect of the measurement noise, which can be achieved by using a filtering technique and signal averaging with more measured series.

In all cases, the inverse of the coefficient matrix $\mathbf{A}$ of the normal equation $\mathbf{AP} = \mathbf{B}$ must be computed to obtain the parameter matrix $\mathbf{P}$. For Cases A and B, the dimension of $\mathbf{A}$ is 4×4 and the numerical accuracy is warrantable. But for Case C, the number of unknowns is 11 and an 11×11 matrix inverse must be computed in the estimation procedure. The parameters of the rotor (m_1^r, c_1^e, k_1^e) are estimated together with those of the bearing. However, in this simulation example, the values of m_1^r and $c_1^e (m_1^r = 6.1 \times 10^{-4}$ Kg and $c_1^e = 1.1 \times 10^{-1}$ Nsm^{-1}) are very small compared with the other terms and this may result in an extremely ill-conditioned matrix when noise is added. This situation explains why the estimated parameter in Table 3 are sensitive to noise even when signal averaging is used. Although this is not shown by the results presented here, we found that the larger the values of m_1^r and c_1^e are, the more accurate the parameter estimates are.

Since it is difficult to measure the defection angles in practice, Case A corresponds more closely to a practical implementation. An experimental test was carried out to illustrate the capability of the estimator for Case A.

7. EXPERIMENTAL SET-UP AND RESULTS

The test rotor-bearing system is shown schematically in Fig. 7. It consisted of a uniform shaft with a disk supported by two standard deep groove ball bearings. The shaft was made of 4140 steel and the disk was made of stainless steel. The support force provided by the ball bearing was purely elastic; that is, the force was produced by elastic contact deformation of the balls, the race, and the local bearing housing structure. An extension was built at the inner ring of each ball bearing, which contained two setscrews to avoid sliding between the contact surfaces of the inner ring and the shaft. By using this design, we could move the bearings along the shaft easily and install the bearings flexibly and conveniently. The bearing pedestals and sensor supports were made of aluminum-alloy and bolted to a steel plate. Each bearing pedestal and sensor support contained two threaded holes in the horizontal and vertical directions to install the proximity probes to detect the displacements of journal motion in the x and y directions. The sensor supports were placed in positions corresponding to the nodes of the finite element model (see Fig. 7). Since a precise value of Young's modulus for 1440 steel was not found in handbooks, a tensile test was performed on the INSTRON 8501. From the readings of the indicators of the strain gage and INSTRON, we obtained the Young's modulus by the equation $E = P/(\varepsilon A)$, where P and ε were increments of load and strain and A was the cross-sectional area of the tensile specimen. The shaft was connected through a flexible coupling to a d-c motor, which can be controlled to maintain a selected speed within ± 1 rpm. The spin speed can be read from the indicator of the dc motor. The disk was fixed by two setscrews and contained a series of axial threaded holes all located at the same distance from its center. These holes could receive balancing/unbalancing masses. The residual unbalance caused by the manufacturing process was not measured, since it was not used in our estimator. The main parameters of the test structure are listed in Table 4.

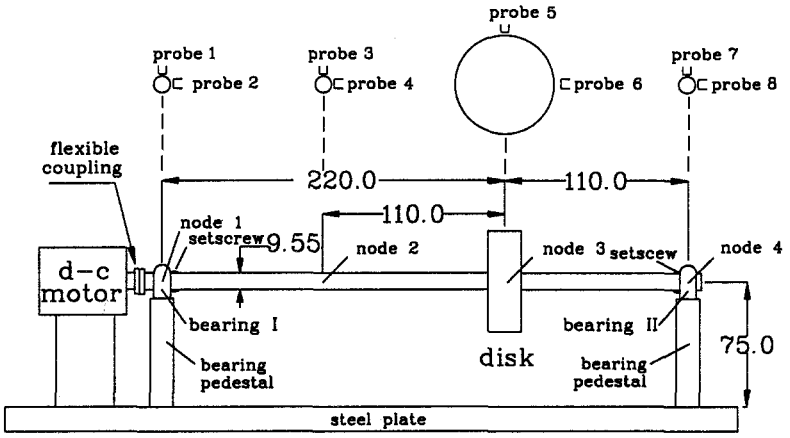

Fig. 7. The experimental rotor-bearing system.

Table 4. Main parameters of the test structure

Shaft		
	material:	4140 steel
	diameter:	9.55 mm
	length L:	330 mm
	Young's modulus E:	2.3×10^{11} Nm^{-2}
	density ρ^e:	7466 kg m^{-3}
Disk		
	material:	stainless steel
	mass m^d:	840 g
	diametric mass moment of inertia I^d:	3.515×10^{-4} kg·m^2
	polar mass moment of inertia J^d:	6.086×10^{-4} kg·m^2

The x, y displacements of the journal motion were detected by the displacement probes. The displacement transducer system used was composed of eight sets of eddy current type noncontacting probes and amplifiers (proximetors). The nominal sensitivity of the proximetor system was 200 and 270 mV/mil for 4140 and stainless steel, respectively. To obtain accurate measurements, we calibrated the sensitivity of each proximetor between measured intervals (8–12 V). An IBM PC, which contained an IEEE-488 interface board for connecting the MICROLINK interface (made by Biodata Ltd.), was chosen for data acquisition. The MICROLINK interface allows flexible interchange of data between transducers and a microcomputer that has the ability to act as controller of the IEEE-488 bus. In the MICROLINK system, the full-scale input range of the analog-to-digital converter modulus was set to 0–10.24 V. The resolution of the A/D converter was 12-bit, i.e. the quantum was 2.5 mV (10.24/4096). Since the maximum value of acceptable signals of the MICROLINK was 10 V, an electrical circuit board was used to reduce the voltage of signals from the proximetor to the MICROLINK (8 V in the experiment). A schematic of the experimental instrumentation is shown in Fig. 8.

Since the finite element technique can provide an accurate simulation of the rotor-bearing system [11], the underlying system was analyzed by three elements and four nodes, of which two bearings were located at nodes 1 and 4 and the disk at node 3, as shown in Fig. 7. In our finite element model, the disk was assumed to be rigid and treated as a node. The diametric and polar mass moments of inertia were computed by $J = mr^2/2$ and $I = mr^2/4 + md^2/12$, where m, r, and d were the mass, radius, and width of the disk, respectively. As the purpose of the test program was to verify the capability of the proposed estimator, the characteristics of the bearing were estimated by two close spin speeds and compared by two different unbalance conditions. Potential errors were introduced by the clearances of the bearings, the misalignment of the shaft, and the circularities of the measured surfaces of the shaft and the disk. To reduce the NSR and enlarge the strength of the signals, the response measurements were taken at spin speeds as close as possible to the first critical speed frequency (4440 rpm) to estimate the bearing characteristics. The sampling frequency was 2 kHz, which was more than ten times the first natural frequency (74 Hz) to avoid the effect of aliasing.

The displacements in the x and y directions from nodes 1 to 4 (x_i, y_i, $i = 1, 2, 3, 4$) were measured by eight proximity sensors at 4045 and 4076 rpm, respectively. Figure 9 shows the typical measurements (x_3) at 4045 rpm when the unbalance mass was not added to the disk; the amplitude of the signal was about 0.1 mm. This amplitude was large enough compared with the maximum static discrepancy (0.01 mm), which was measured by slowly rotating the shaft in one revolution. Applying a Fourier transform to the eight records of each sin speed [$x_i(k)$, $y_i(k)$, $i = 1, 2, 3, 4$, $k = 1024$], we can obtain the coefficients x_{ic}, x_{is}, y_{ic}, and y_{is}. By using Eqns (28–29), we can compute matrices $\mathbf{A}_1$, $\mathbf{A}_2$, $\mathbf{B}_1$, and $\mathbf{B}_2$ in Eqn (24) to estimate the parameter martrix $\mathbf{P}$. A number of tests were performed on the laboratory set-up. In

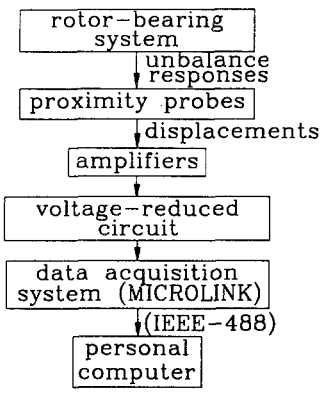

Fig. 8. Schematic of experimental instrumentation.

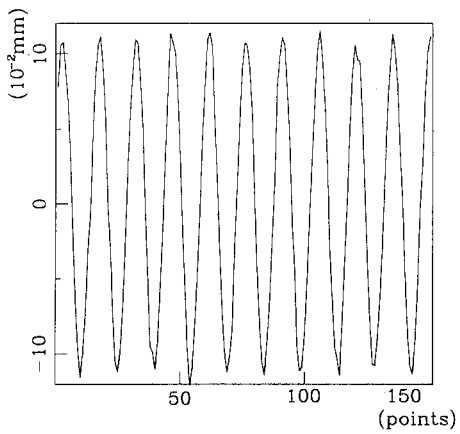

Fig. 9. Typical experimental responses.

particular, regarding the model response to unbalance, two configurations were considered: the first one had no setscrews used as unbalance masses in the disk mass; the second had setscrews (total mass: 1.9×10^{-3} Kg) placed in a sector of the disk mass. The characteristics of the two ball bearings were then obtained, as shown in Table 5. Since the unbalance mass added was small compared with the mass of the disk, the disk mass and gyroscopic matrices (M^d and G^d) in Eqn (8) can be assumed to be unchanged. The main effect was the synchronous unbalance forces with magnitude $md\Omega^2$ (m is the mass of the unbalance, d the distance of the unbalance mass from the center, and Ω the spin speed). From Table 5 we find that the estimated parameters were consistent for these two unbalance conditions.

Because there is no standard, reliable method for determining the exact parameters, it is difficult to judge how to verify the accuracy of the results identified by the proposed method. However, the bearing stiffness and damping can be verified indirectly by employing the estimated coefficients in the finite-element model, which predicts the frequency response characteristics of the rotor-bearing system. This prediction can then be compared with frequency responses measured on the actual system. The impact excitation test was adopted here to obtain the frequency response function (FRF) of the machine to verify the accuracy of the estimates. The impulse force was generated by an ICP impulse-force hammer, which was made by PCB Piezotronics, Inc. The hammer impacted the rotor through a piezo-electric force transducer and a relative soft and curve cap, the selected cap material being a compromise between the required frequency response span and the ability to withstand

Table 5. Estimation results from experimental data

$k^b_{xx}(10^8\,\mathrm{Nm^{-1}})$	$k^b_{xy}(10^2\,\mathrm{Nm^{-1}})$	$k^b_{yx}(10^2\,\mathrm{Nm^{-1}})$	$k^b_{yy}(10^8\,\mathrm{Nm^{-1}})$
Unbalance masses not added			
br. I 1.67	1.15	1.65	1.54
br. II 1.46	1.07	1.26	1.31
Some unbalance masses added			
br. I 1.69	1.13	1.61	1.55
br.. II 1.44	1.10	1.23	1.27
$c^b_{xx}(10^2\,\mathrm{Nsm^{-1}})$	$c^b_{xy}(10^1\,\mathrm{Nsm^{-1}})$	$c^b_{yx}(10^1\,\mathrm{Nsm^{-1}})$	$c^b_{yy}(10^2\,\mathrm{Nsm^{-1}})$
Unbalance masses not added			
br. I 3.34	8.91	5.71	4.66
br. II 3.14	7.89	5.01	4.44
Some unbalance masses added			
br. I 3.31	8.87	5.76	4.67
br.. II 3.18	7.93	5.04	4.41

the sliding speeds of the rotor without being worn flat too quickly. The nominal sensitivity of the hammer was 2.12 mV/N. The displacements were detected by the displacement probe as before. We then obtained the FRF of the machine by analyzing the impact force and response signals by a multichannel spectrum analyzer (FFT), made by Schlumberger Technologies. The schematic of the impact excitation test is shown in Fig. 10.

The frequency response functions, generally speaking, were speed dependent because of two not easily separated causes: the variable stiffness and damping of the rolling element bearings, and the influence of gyroscopic moments. When the unbalance mass was not added to the disk, the frequency response function at 4045 spin speed obtained by impacting the disk in the horizontal direction and measuring the displacement in the same direction was as shown in Fig. 11. From Fig. 11 we find that the first natural frequency was about 74 Hz and there was no apparent split frequency. Although the rotor was balanced as well as possible, there was a strong component at 67 Hz, which was caused by the existing unbalance in the rotor. The other small peaks were caused by the bearing pedestals, the sensor supports and the local foundation plate resonances. Another potential error was introduced by the friction between the impact head and the rotating shaft (and the "smearing-out" of the impact force).

By using the estimated stiffness and damping coefficients of bearings in the finite-element model, we found that the first critical speed was split into two values, i.e. 70.925 and 72.015 Hz at 4045 rpm spin speed, which were obtained by computing the eigenvalues of the characteristic matrix of the model. For 4076 rpm spin speed, we obtained 70.921 and 72.019 Hz, which were close to the values obtained at 4045 rpm. The split effects were due to the gyroscopic effect caused by the mass moment inertia of the shaft and the disk. The

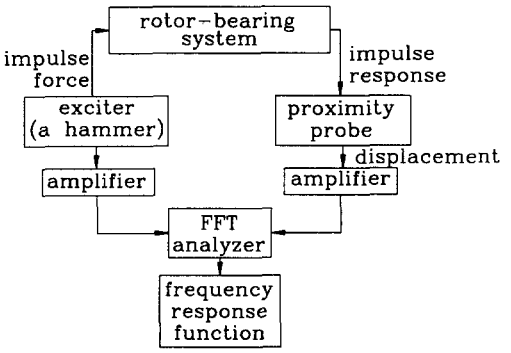

Fig. 10. Schematic of impact excitation test.

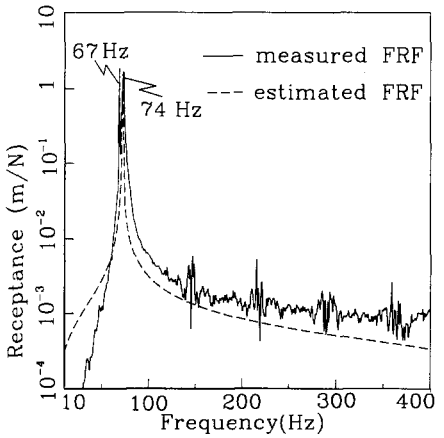

Fig. 11. Comparison of frequency response functions between the machine and the estimated model.

estimated first natural frequencies were close to that of the machine obtained from the experimental force vibration (74 Hz). Employing the estimated bearing parameters in the model represented by Eqn (10), we can obtain the estimated FRF, which is represented by the dashed line in Fig. 11. No split peaks are apparent since the two frequencies were too close. Comparing the FRFs obtained from the estimated model and the machine, we find they were close to each other and the estimated bearing characteristics can be regarded as accurate.

8. CONCLUSION

The present paper proposes a new method of identifying linearized bearing characteristics based on a finite element formulation. Unlike previous methods, the present method treats the rotor as flexible and thus better reflects most practical situations. The present method also eliminates the need to obtain all of the characteristics of the rotor or measure synchronous forces. From Cases A to C we find that the constant matrices **A** and **B** in the normal equation $\mathbf{A}\hat{\mathbf{P}} = \mathbf{B}$ are functions of the coefficients which are determined by applying a Fourier transform to displacements. Thus the effects of measurement noise and random system disturbances are automatically filtered out except for the noise component at the rotational frequency. Noise reduction can be further enhanced by signal averaging. Comparing the results in Tables 1, 2 and 3, we see that the greater the amount of information available on the rotor-bearing system, the less sensitive to noise the estimate becomes. Since it is difficult to measure the deflection angle in practice, the method in Case A is more applicable to practical implementations. The main conclusions of this paper can be summarized as follows:

(1) When all the characteristics of the shaft and disks are known (Case A), the responses about the deflection angle can be replaced by deflection, but the responses of deflections (x_i, y_i) at all nodes must be measured to estimate the bearing parameters.

(2) When the characteristics of segments located in the vicinity of the bearing to be estimated are known, e.g. the characteristics of segment 1 are known when bearing 1 is to be estimated (Case B), the method described in Section 4 can be used. In this case, the measurements are the responses of nodes 1 and 2 $(x_1, y_1, \theta_{y1}, \theta_{x1}, x_2, y_2, \theta_{y2}, \theta_{x2})$.

(3) When the characteristics of the rotor are unknown except for the mass of a segment located in the vicinity of the bearings to be estimated, e.g. when bearing 1 is to be estimated and the mass of segment 1, m_1^s, is known (Case C), the responses of nodes 1 and 2 $(x_1, y_1, \theta_{y1}, \theta_{x1}, x_2, y_2, \theta_{y2}, \theta_{x2})$ can be used to estimate the parameters of the bearing by the method described in Section 5. Since the parameters of the rotor (m_1^r, c_1^e, k_1^e) are estimated together with those of the bearing, the dimension of the coefficient matrix **A** in the normal equation is (11×11), and the sensitivity to noise is high compared with Cases A and B.

Acknowledgements—This study was supported by the National Science Council, Republic of China, under contract number NC 81-0401-E-009-08.

REFERENCES

1. C. R. Burrows and R. Stanway, Identification of Journal Bearing Characteristics. *ASME J. Dyn. Syst. Meas. Control* **99**, 167 (1977).
2. R. Stanway, C. R. Burrows and R. Homes, Discrete Time Modeling of Squeeze Film Bearing. *J. Mech. Engng. Sci.* **21**(6), 419 (1979).
3. C. R. Burrows and M. N. Sahinkaya, Frequency Domain Estimation of Linearized Oil-Film Coefficients. *ASME J. Lubric. Tech.* **104**, 210 (1982).
4. R. Stanway, Identification of Linearized Squeeze-Film Dynamics Using Synchronous Excitation. *Proc. Instn. Mech. Engrs* **197C**, 199 (1983).
5. M. N. Sahinkaya and C. R. Burrows, Estimation of Linearized Oil Film Parameters from the Out of Balance Response. *Proc. Instn. Mech. Engrs* **198**(C8), 107 (1984).
6. C.W. Lee and S. W. Hong, Identification of Bearing Dynamic Coefficients by Unbalance Response Measurements. *Proc. Instn. Engrs* **203**, 93 (1989).
7. S. I Kim and B. M. Kwak, Identification of Bearing Coefficients by Incomplete Mode Shapes. *Mechanical System and Signal Processing* **4**(5), 425 (1990).

8. C. W. Lee and Y. G. Jei, Modal Analysis of Continuous Rotor-Bearing System. *J. Sound Vibr.* **126**(2), 345 (1988).
9. L. Meirovitch, *Computational Methods in Structural Dynamics*, Sijthoff and Noordhoff, The Netherlands (1980).
10. H. D. Nelson and J. M. Mcvaugh, The Dynamics of Rotor-Bearing Systems Using Finite Elements. *ASME J. Engng. Industry* **98**, 593 (1976).
11. Y. Kang, Y. P. Shih and A. C. Lee, Investigation of the Steady-state Responses of Asymmetric Rotors *ASME J. of Vibr. Acoust.* **114**, 194 (1992).

APPENDIX A: LOCAL MATRICES

$$\mathbf{L}_s = \int_0^1 (\phi_x \phi_x^t + \phi_y \phi_y^t)\,\mathrm{d}\xi$$

$$= \begin{bmatrix} .37143 & 0 & .05238 & 0 & .12857 & 0 & -.03095 & 0 \\ 0 & .37143 & 0 & -.05238 & 0 & .12857 & 0 & .03095 \\ .05238 & 0 & .00952 & 0 & .03095 & 0 & -.00714 & 0 \\ 0 & .05328 & 0 & .00952 & 0 & -03095 & 0 & -.00714 \\ .12857 & 0 & .03095 & 0 & .37143 & 0 & -.05238 & 0 \\ 0 & .12857 & 0 & .03095 & 0 & .37143 & 0 & .05238 \\ -.03095 & 0 & -.00714 & 0 & -.05238 & 0 & 00952 & 0 \\ 0 & \cdot 03095 & 0 & -.00714 & 0 & .05238 & 0 & \cdot 00952 \end{bmatrix}$$

$$\mathbf{L}_r = \int_0^1 (\phi_x' \phi_x'' + \phi_y' \phi_y'')\,\mathrm{d}\xi$$

$$= \begin{bmatrix} 1.2000 & 0 & .10000 & 0 & -1.2000 & 0 & .10000 & 0 \\ 0 & 1.2000 & 0 & -.10000 & 0 & -1.2000 & 0 & -.10000 \\ .100000 & 0 & .13333 & 0 & -.10000 & 0 & -.03333 & 0 \\ 0 & -.10000 & 0 & .13333 & 0 & .10000 & 0 & -.03333 \\ -1.2000 & 0 & -.10000 & 0 & 1.2000 & 0 & -.10000 & 0 \\ 0 & -1.2000 & 0 & .10000 & 0 & 1.2000 & 0 & .10000 \\ .10000 & 0 & -.03333 & 0 & -.10000 & 0 & .13333 & 0 \\ 0 & 0.10000 & 0 & -.03333 & 0 & .10000 & 0 & .13333 \end{bmatrix}$$

$$\mathbf{L}_c = \int_0^1 (\phi_y' \phi_x'' - \phi_x' \phi_y'')\,\mathrm{d}\xi$$

$$= \begin{bmatrix} 0 & -1.2000 & 0 & .10000 & 0 & 1.2000 & 0 & .10000 \\ 1.2000 & 0 & .10000 & 0 & -1.2000 & 0 & .10000 & 0 \\ 0 & -.10000 & 0 & .13333 & 0 & .10000 & 0 & -.03333 \\ -.10000 & 0 & -13333 & 0 & .10000 & 0 & ,03333 & 0 \\ 0 & 1.2000 & 0 & -.10000 & 0 & -1.2000 & 0 & -.10000 \\ -1.2000 & 0 & -.10000 & 0 & 1.2000 & 0 & -.10000 & 0 \\ 0 & -.10000 & 0 & -.03333 & 0 & .10000 & 0 & .13333 \\ -.10000 & 03095 & .33333 & & .10000 & 0 & -.13333 & 0 \end{bmatrix}$$

$$\mathbf{L}_k = \int_0^1 (\phi_x'' \phi_x''' + \phi_y'' \phi_y''') \, d\xi$$

$$= \begin{bmatrix} 12 & 0 & 6 & 0 & -12 & 0 & 6 & 0 \\ 0 & 12 & 0 & -6 & 0 & -12 & 0 & -6 \\ 6 & 0 & 4 & 0 & -6 & 0 & 2 & 0 \\ 0 & -6 & 0 & 4 & 0 & 6 & 0 & 2 \\ -12 & 0 & -6 & 0 & 12 & 0 & -6 & 0 \\ 0 & -12 & 0 & 6 & 0 & 12 & 0 & 6 \\ 6 & 0 & 2 & 0 & -6 & 0 & 4 & 0 \\ 0 & -6 & 0 & 2 & 0 & 6 & 0 & 4 \end{bmatrix}$$

APPENDIX B: DERIVATION OF THE MATRICES E, F, G, H, $\mathbf{w}_c$, $\mathbf{w}_s$, $\mathbf{f}_{ac}$, $\mathbf{f}_{as}$ IN SECTION 3

Substituting Eqns (16–17) into Eqn (15), one obtains

$$\begin{aligned} &- \Omega^2 m_{\theta z}(z_c \cos \Omega t + z_s \sin \Omega t) - \Omega^2 m_{\theta\theta}(\theta_c \cos \Omega t + \theta_s \sin \Omega t) \\ &+ \Omega c_{\theta z}(z_s \cos \Omega t + z_c \sin \Omega t) + \Omega c_{\theta\theta}(\theta_s \cos \Omega t - \theta_c \sin \Omega t) \\ &+ k_{\theta z}(z_c \cos \Omega t + z_s \sin \Omega t) + k_{\theta\theta}(\theta_c \cos \Omega t + \theta_s \sin \Omega t) = 0 \end{aligned} \tag{B1}$$

Reorganizing Eqn (B1) by sine and cosine terms and setting them equal to zero individually, we obtain the following equations:

$$(-\Omega^2 m_{\theta z} + k_{\theta z}) z_c + \Omega c_{\theta z} z_s + (-\Omega^2 m_{\theta\theta} + k_{\theta\theta}) \theta_c + \Omega c_{\theta\theta} \theta_s = 0 \tag{B2}$$

$$(-\Omega^2 m_{\theta z} + k_{\theta z}) z_s - \Omega c_{\theta z} z_c + (-\Omega^2 m_{\theta\theta} + k_{\theta\theta}) \theta_s + \Omega c_{\theta\theta} \theta_c = 0 \tag{B3}$$

Solving Eqns (B2) and (B3), we obtained θ_c and θ_s as follows:

$$\theta_c = \mathbf{E} z_c + \mathbf{F} z_s \tag{B4}$$

$$\theta_s = \mathbf{G} z_c + \mathbf{H} z_s \tag{B5}$$

where

$$\mathbf{E} = [c_{\theta\theta}^{-1}(k_{\theta\theta} - \Omega^2 m_{\theta\theta})/\Omega + \Omega(k_{\theta\theta} - \Omega^2 m_{\theta\theta})^{-1} c_{\theta\theta}]^{-1} \cdot [c_{\theta\theta}^{-1}(k_{\theta z} - \Omega^2 m_{\theta z})/\Omega + \Omega(k_{\theta\theta} - \Omega^2 m_{\theta\theta})^{-1} c_{\theta z}]$$

$$\mathbf{F} = [c_{\theta\theta}^{-1}(k_{\theta\theta} - \Omega^2 m_{\theta\theta})/\Omega + \Omega(k_{\theta\theta} - \Omega^2 m_{\theta\theta})^{-1} c_{\theta\theta}]^{-1} \cdot [c_{\theta\theta}^{-1} c_{\theta z} - (k_{\theta\theta} - \Omega^2 m_{\theta\theta})^{-1}(k_{\theta z} - \Omega^2 m_{\theta z})]$$

$$\mathbf{G} = [c_{\theta\theta}^{-1}(k_{\theta\theta} - \Omega^2 m_{\theta\theta})/\Omega + \Omega(k_{\theta\theta} - \Omega^2 m_{\theta\theta})^{-1} c_{\theta\theta}]^{-1} \cdot [-c_{\theta\theta}^{-1} c_{\theta z} - (k_{\theta\theta} - \Omega^2 m_{\theta\theta})^{-1}(k_{\theta z} - \Omega^2 m_{\theta z})]$$

$$\mathbf{H} = [c_{\theta\theta}^{-1}(k_{\theta\theta} - \Omega^2 m_{\theta\theta})/\Omega + \Omega(k_{\theta\theta} - \Omega^2 m_{\theta\theta})^{-1} c_{\theta\theta}]^{-1} \cdot [c_{\theta\theta}^{-1}(k_{\theta z} - \Omega^2 m_{\theta z})/\Omega + \Omega(k_{\theta\theta} - \Omega^2 m_{\theta\theta})^{-1} c_{\theta z}]$$

Substituting Eqns (B4–B5) into Eqn (17), one obtains:

$$\theta(t) = (\mathbf{E} z_c + \mathbf{F} z_s) \cos \Omega t + (\mathbf{G} z_c + \mathbf{H} z_s) \sin \Omega t \tag{B6}$$

Then, substituting Eqns (B6) and (16) into Eqn (14), we can obtain the following equation:

$$\begin{aligned} &[c_{zz}^b k_{zz}^b] \left(\begin{bmatrix} -z_s \\ z_c \end{bmatrix} \cos \Omega t + \begin{bmatrix} -z_c \\ z_s \end{bmatrix} \sin \Omega t \right) = \\ &- \{[(-\Omega^2 m_{zz} + k_{zz}) + (-\Omega^2 m_{z\theta} + k_{z\theta})\mathbf{E} + \Omega c_{z\theta} \mathbf{G}] z_c \\ &+ [\Omega c_{zz} + (-\Omega^2 m_{z\theta} + k_{z\theta})\mathbf{F} + \Omega c_{z\theta} \mathbf{H}] z_s\} \cos \Omega t \\ &- \{[(-\Omega^2 m_{zz} + k_{zz}) + (-\Omega^2 m_{z\theta} + k_{z\theta})\mathbf{H} + \Omega c_{z\theta} \mathbf{F}] z_s \\ &+ [-\Omega c_{zz} + (-\Omega^2 m_{z\theta} + k_{z\theta})\mathbf{G} + \Omega c_{z\theta} \mathbf{E}] z_c\} \sin \Omega t \end{aligned} \tag{B7}$$

Extract the first and $(n+2)$'th rows of Eqn (B7) and take the transpose of both sides. Equation (20) can be obtained as follows:

$$(w_c^t \cos \Omega t + w_s^t \sin \Omega t)\mathbf{P} = f_{ac}^t \cos \Omega t + f_{as}^t \sin \Omega t$$

where

$$w(t) = [\dot{x}_1(t), \dot{y}_1(t), x_1(t), y_1(t)]^t = (w_c \cos \Omega t + w_s \sin \Omega t)$$

$$\mathbf{P}^t = \begin{bmatrix} c_{xx1}^b & c_{xy1}^b & k_{xx1}^b & k_{xy1}^b \\ c_{yx1}^b & c_{yy1}^b & k_{yx1}^b & k_{yy1}^b \end{bmatrix} = [\mathbf{C}_1^b \ \mathbf{K}_1^b]$$

and $\mathbf{f}_{ac}$, $\mathbf{f}_{as}$ are 2×1 vectors which contain the first and $(n+2)$'th rows of coefficient matrices of the cosine and sine terms, respectively, for the right-hand side of Eqn (B7).

APPENDIX C: DETAILS of a_i

$$a_1 = (\partial \mathbf{D}/\partial c^{b}_{xx1})\mathbf{W}(t) = [\dot{x}_1 \ 0]^t \quad a_2 = (\partial \mathbf{D}/\partial c^{b}_{xy1})\mathbf{W}(t) = [\dot{y}_1 \ 0]^t$$

$$a_3 = (\partial \mathbf{D}/\partial c^{b}_{yx1})\mathbf{W}(t) = [0 \ \dot{x}_1]^t \quad a_4 = (\partial \mathbf{D}/\partial c^{b}_{yy1})\mathbf{W}(t) = [0 \ \dot{y}_1]^t$$

$$a_5 = (\partial \mathbf{D}/\partial k^{b}_{xx1})\mathbf{W}(t) = [x_1 \ 0]^t \quad a_6 = (\partial \mathbf{D}/\partial k^{b}_{xy1})\mathbf{W}(t) = [y_1 \ 0]^t$$

$$a_7 = (\partial \mathbf{D}/\partial k^{b}_{yx1})\mathbf{W}(t) = [0 \ x_1]^t \quad a_8 = (\partial \mathbf{D}/\partial k^{b}_{yy1})\mathbf{W}(t) = [0 \ y_1]^t$$

$$a_9 = (\partial \mathbf{D}/\partial m^{r}_1)\mathbf{W}(t) = \mathbf{L}^*_r \ddot{\mathbf{q}}^e_1 \qquad a_{10} = (\partial \mathbf{D}/\partial c^{e}_1)\mathbf{W}(t) = \mathbf{L}^*_c \dot{\mathbf{q}}^e_1$$

$$a_{11} = (\partial \mathbf{D}/\partial k^{e}_1)\mathbf{W}(t) = \mathbf{L}^*_k q^e_1$$

APPENDIX D: DETAILS OF MODIFIED a_i

$$a_1 = (\partial \mathbf{D}/\partial c^{b}_{xx1})\mathbf{W}(t) = [\dot{x}_1 \ 0 \ 0 \ 0]^t \quad a_2 = (\partial \mathbf{D}/\partial c^{b}_{xy1})\mathbf{W}(t) = [\dot{y}_1 \ 0 \ 0 \ 0]^t$$

$$a_3 = (\partial \mathbf{D}/\partial c^{b}_{yx1})\mathbf{W}(t) = [0 \ \dot{x}_1 \ 0 \ 0]^t \quad a_4 = (\partial \mathbf{D}/\partial c^{b}_{yy1})\mathbf{W}(t) = [0 \ \dot{y}_1 \ 0 \ 0]^t$$

$$a_5 = (\partial \mathbf{D}/\partial k^{b}_{xx1})\mathbf{W}(t) = [x_1 \ 0 \ 0 \ 0]^t \quad a_6 = (\partial \mathbf{D}/\partial k^{b}_{xy1})\mathbf{W}(t) = [y_1 \ 0 \ 0 \ 0]^t$$

$$a_7 = (\partial \mathbf{D}/\partial k^{b}_{yx1})\mathbf{W}(t) = [0 \ x_1 \ 0 \ 0]^t \quad a_8 = (\partial \mathbf{D}/\partial k^{b}_{yy1})\mathbf{W}(t) = [0 \ y_1 \ 0 \ 0]^t$$

$$a_9 = (\partial \mathbf{D}/\partial m^{r}_1)\mathbf{W}(t) = \mathbf{L}^{\#}_r \ddot{\mathbf{q}}^e_1 \qquad a_{10} = (\partial \mathbf{D}/\partial c^{e}_1)\mathbf{W}(t) = \mathbf{L}^{\#}_c \dot{q}^e_1$$

$$a_{10} = (\partial \mathbf{D}/\partial k^{e}_1)\mathbf{W}(t) = \mathbf{L}^{\#}_r \ddot{\mathbf{q}}^e_1$$

APPENDIX E: CONTRIBUTION OF THE VELOCITY TERM IN EQUATION (34)

From Appendix A, the local matrices $\mathbf{L}^*_s$, L^*_r, $\mathbf{L}^*_c$, and $\mathbf{L}^*_k$ have the same order of magnitude; let us set them to be $\mathbf{L}$. Since the rotor-bearing system is in the steady state, with spin speed Ω, the magnitude of the acceleration is $\Omega^2 w$ and that of the velocity is $\Omega \mathbf{w}$ (where $\mathbf{w}$ denotes general deflection). Then, each term on the right-hand side of Eqn (34) can be approximated as

$$|(m^s_1 + m^r_1)\mathbf{L}^*_r \ddot{\mathbf{w}}| \simeq \Omega^2(l\rho^e A^e + \rho^e I^e/l)\mathbf{L}\mathbf{w} \tag{E1}$$

$$|c^e_1 \mathbf{L}^*_c \dot{\mathbf{w}}| \simeq (\Omega^2 J^e/l^2)\mathbf{L}\mathbf{w} \tag{E2}$$

$$|k^e_1 \mathbf{L}^*_k \mathbf{w}| \simeq (E^2 I^e/l^3)\mathbf{L}\mathbf{w} \tag{E3}$$

Taking the ratio of Eqns (E1), (E2) and (E3), we have

$$[\Omega^2(l\rho^e A^e + \rho^e I^e/l)]: (\Omega^2 J^e/l^2): (E I^e/l^3)$$

$$= \frac{\Omega^2 \rho^e I^e (16l/d^2 + 1/l)}{(2\Omega^2 \rho^e l/l^2)} : 1 : [E/(2\Omega^2 l)]$$

$$= [8(l/d)^2 + 0.5] : 1 : [E/(2\Omega^2 l)] \tag{E4}$$

where l is the length of the segment and d the diameter of the shaft. In general, Young's modulus is very large, so if $l > d$, the contribution of the velocity term can be neglected compared with the other terms on the right-hand side of Eqn (34).